Kinetic Molecular Cationic Control of Defect-Induced Broadband Light Emission in 2D Hybrid Lead Iodide Perovskites

Adedayo M. Sanni and Aaron S. Rury*

Department of Chemistry, Wayne State University, Detroit, MI, USA 48202

E-mail: aaron.rury@wayne.edu

Abstract

In this study we examine the effects of changing organic cation concentrations on the efficiency and photophysical implications of exciton trapping in 2-dimensional hybrid lead iodide self-assembled quantum wells (SAQWs). We show increasing the concentration of alkyl and aryl ammonium cations causes the formation of SAQWs at a liquid-liquid interface to possess intense, broadband subgap photoluminescence (PL) spectra. Electron microscopy, X-ray diffraction, and X-ray photoelectron spectroscopic studies suggest materials formed under these cation concentrations possess morphologies consistent with inhibited crystallization kinetics, but exhibit qualitatively similar bulk chemical bonding to non-luminescent materials stabilized in the same structure from precursor solutions containing lower cation concentrations. Temperature and power-dependent PL spectra suggest the broadband subgap light emission stems from excitons self-trapped at defect sites, which we assign as edge-like, collective I^- vacancies using a simple model of the chemical equilibrium driving material self-assembly. These results suggest changes to the availability of molecular cations can suitably control the light emission properties of self-assembled hybrid organic-inorganic materials in ways central to their applicability in lighting technologies.

1

The luminescent properties of self-assembled, excitonic nanomaterials formed from organic and inorganic constituents remain an area of intense research interest. This interest stems in large part from two characteristics of these materials. First, one can form highly luminescent materials from solvated chemical precursors at or near room temperature. Second, the size of these materials increases the prospects of interfacing them with interconnects in nano- and microscopic optoelectronic devices as white-light sources,[1–3] light emitting diodes[4–7] and lasers.[5] Despite these prospects, the chemical control of all light emission properties in this class of materials remains incomplete. In the case of photoluminescence (PL) below the exciton gap of hybrid organic-lead iodide self-assembled quantum wells (SAQWs), the lack of clear chemical means to control light emission inhibits assignments of the physical mechanism controlling these processes and the development of these materials as light sources for near-IR sensing technologies in security and imaging applications.

Hybrid SAQWs form from the self-assembly of sheets comprised of main group metal-halide octahedra spaced by layers of intercalated molecular cations.[8–11] Significant confinement of the electron and hole drives the formation of excitons in hybrid SAQW samples whose binding energy often exceeds 100 meV and leads to narrow, efficient PL stemming from recombination.[12] In addition to this intense light emission assigned to the recombination of the free exciton, several studies report the appearance of PL caused by the recombination of trapped excitons and individual charge carriers.[13–19] Despite this broad assignment, the characteristics of the spectra emitted by hybrid SAQW samples vary with many conditions, even for the same chemical compound. For example, various group report different subgap PL spectra depending on the sample structure and morphology of hexyl ammonium lead iodide (HA_2PbI_4). In particular, while Booker et al.[20] report a relatively weak subgap PL feature centered at 650 nm and possessing a bandwidth of 150 nm emitted by thin films of HA_2PbI_4 in its orthorhombic *Pbca* phase, Sanni et al.[18] report a significantly more intense spectrum centered at 750 nm and possessing a nearly 300 nm bandwidth in single crystals of this material in its monoclinic *P2$_1$c* structure.

Researchers propose these spectra can stem from both local chemical and macroscopic, mor-

phological differences between SAQW samples. For example, recent studies suggest similar sub-gap PL spectra can be caused by chemical impurities such as metal and halide interstitials and vacancies,[13,16–19,21] solution impurities,[22] and exciton self-trapping induced by molecular cations.[1,3,23–25] In addition, other studies indicate the presence of electronic states on the edges and dislocations of crystals correlate with broadband, subgap light emission from SAQW samples possessing the Ruddlesden-Popper structure.[26–28] Given the variation in experimental observations of the characteristics of subgap PL from hybrid SAQWs with so many different parameters of material formation, the general understanding of the mechanisms by which different types of electronic states participate in the trapping and recombination of excitons and charge carriers remains incomplete. For instance, researchers still do not understand whether the broadband light emission stems from excitonic states thought to dominate the electronic structure of hybrid-SAQWs or from charge carriers formed following direct excitation into these materials' conduction bands. Part of this knowledge gap stems from the lack of a complete set of chemical methods to control the presence and characteristics of the subgap PL spectra.

Studies indicate controlling the inorganic chemicals in precursor solutions can cause important changes to the appearance of subgap PL from hybrid lead iodide SAQWs. In particular, Mitzi and co-workers suggest controlling the presence of Sn impurities in solutions from which phenylethyl ammonium lead iodide (PEA_2PbI_4) SAQWs form acts as a chemical lever to induce the appearance of broadband subgap PL from these materials.[21] These authors use density functional theory (DFT) calculations to propose ultrafast trapping of the hole contribution to the free exciton at Sn impurity sites drive formation of the self-trapped exciton (STE) and emission of a broadband spectrum of light below the exciton energy gap. In addition, Zhang et al. used excess iodine in aqueous precursor solutions to induce broadband subgap PL.[16] Furthermore, Yin et al. show that samples of PEA_2PbI_4 formed from precursor solutions made with PbO do not possess significant broadband subgap PL, while the same material made from aqueous solutions of PbI_2 do possess these spectral features caused by structural defects.[19] Using further chemical treatments of PEAI in combination with DFT calculations these authors suggest the presence of PbI_3^- and PbI_4^{2-} polyiodide species in

their precursor solution drive the formation of I^- vacancies, which trap the electron contribution to the free exciton and allow radiative relaxation below the exciton gap. Despite this progress in the chemical control of broadband emission from hybrid SAQWs, it remains unclear if such methods can be extended to materials beyond PEA_2PbI_4. Moreover, there remain no reports on the role controlling chemical conditions of the organic constituents can play in modulating the subgap PL from these materials.
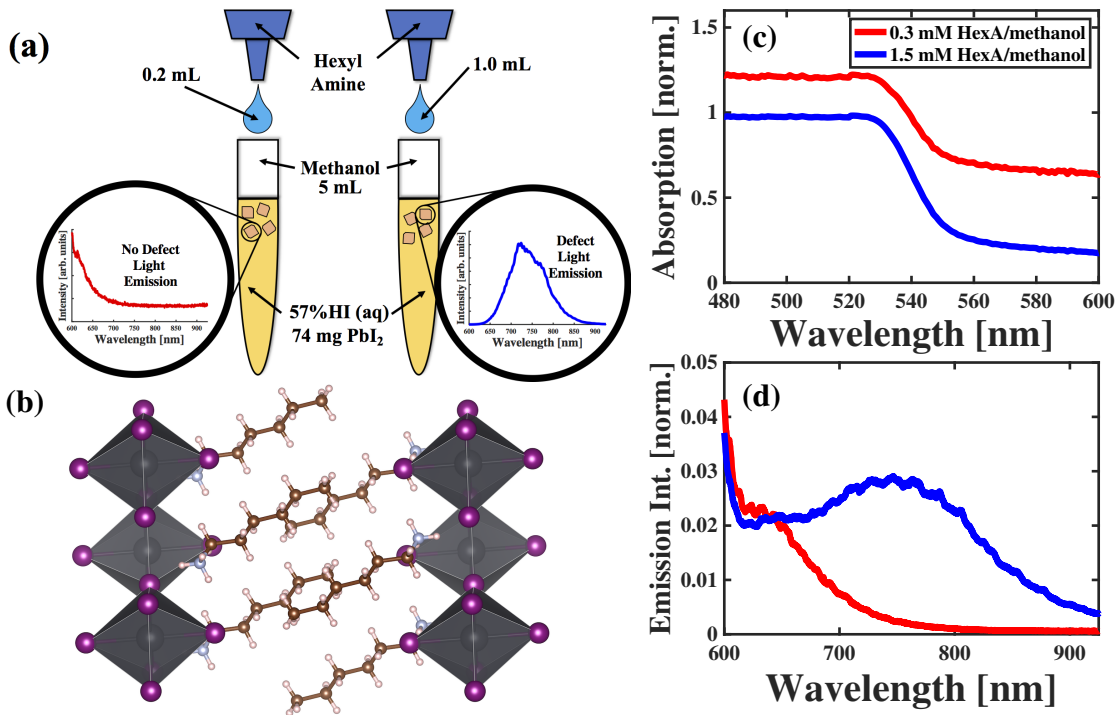

Figure 1: (a) Shows a schematic of the synthetic approaches we use in making hybrid organic lead iodide self-assembled quantum wells (SAQWs) to control the presence of broadband photoluminescence at room temperature. (b) Established structure of our hexyl ammonium lead iodide (HA_2PbI_4) SAQWs obtained from the synthetic approach described in the text. (c) Comparison between room temperature normalized absorption spectrum of a HA_2PbI_4 sample formed using a 0.3 mM HexA/methanol organic solution layer (red) to that of sample formed using a 1.5 mM HexA/methanol organic solution layer. The absorption plots have been offset for clarity. (d) Comparison between the room temperature subgap photoluminescence spectra emitted by HA_2PbI_4 formed using 0.3 mM (red) and 1.5 mM (blue) HexA/methanol organic solution layers.

In this study we report a molecule-forward chemical approach through which we can control the presence of room temperature broadband light emission from several hybrid lead iodide SAQW samples possessing both alkyl and aryl molecular cations. In our synthetic method, we modify a

chemical approach in which one dissolves the organic and inorganic constituents of the hybrid SAQW material in solvents physically separated into layers in a test tube. Formation of a distinct liquid-liquid interface restricts the spatial region in which the self-assembly of the hybrid SAQWs can occur. By modulating the formation of molecular cations at the liquid-liquid interface, we find a means to control the light emission spectra of the resultant materials. Figure 1(a) shows this chemical approach schematically.

As a case study, we begin by assessing the light emission, morphological, and structural properties of hexyl ammonium lead iodide (HA_2PbI_4) formed through our chemical approach. Using the approach described in Methods we form the $P2_1/c$ monoclinic phase of HA_2PbI_4, whose structure is shown in Figure 1(b). When we vary the amount of hexyl amine (HexA) we add to a 5 mL methanol layer in a test tube, we affect the resultant material's photophysical properties in targeted ways. In particular, while Figure 1(c) shows we form HA_2PbI_4 samples whose absorption spectra do not differ significantly by making 0.3 mM HexA/methanol and 1.5 mM HexA/methanol solutions, we find the light emission spectra of materials formed from these different solutions vary substantially. As seen in Figure 1(d), following excitation at 532 nm we find the PL spectrum a HA_2PbI_4 sample formed from the 1.5 mM HexA/methanol solution layer possesses a prominent peak centered at 750 nm, which is conspicuously absent from the spectrum we find emitted by the sample formed from the 0.3 mM HexA/methanol organic layer. The broadband emission from the 1.5 mM HexA/methanol HA_2PbI_4 sample possesses many characteristics of the subgap PL emitted from PEA_2PbI_4 samples reportedly previously.[13,19,21] Most importantly, we find this light emission feature is red-shifted by nearly 200 nm from the narrow photoluminescence emitted due free exciton recombination and possesses the broad bandwidth consistent with PL caused by so-called edge states in mixed cation, Ruddlesden-Popper hybrid perovskites reported by numerous authors.[26-28] Contrasting with previous studies, however, the 532 nm laser in our experiments excites the free exciton directly and allows us determine how the concentrations of molecular constituents in precursor solutions affect the photophysical properties of hybrid SAQWs. In particular, driving the exciton resonantly not only allows us to discount trapping of charge carriers photo-

5

generated promptly with higher energy light, but also allows us to use power-dependent PL spectra and investigate the excited state processes driving subgap PL in our samples, as we discuss in more detail below. In addition to differences in the light emission spectra, the morphologies of the HA_2PbI_4 samples we form from the two organic solutions contrast starkly.

The panels (a)-(d) of Figure 2 compare the scanning electron microscopy (SEM) images of HA_2PbI_4 samples formed from 0.3 mM of HexA/methanol solution layers to those of samples formed by making 1.5 mM HexA/methanol layers. Comparison of these images at both low and high magnification indicates the morphological features in each respective sample differ significantly. In particular, we find the samples formed from the 0.3 mM HexA/methanol organic solvent layers possess platy structures with both smooth surfaces and edges, as seen in the panels (a) and (c) of Figure 2. In contrast, smaller, more granular crystallites with sharper edges comprise the samples we form using the 1.5 mM HexA/methanol solvent layers, as shown in panels (b) and (d) of Figure 2. These differences indicate the crystallization process within the materials' *ab*-planes differs qualitatively as we vary the amount of amine we add to each respective methanol layer.

Panels (e)-(g) of Figure 2 show these differences in the crystallization process also manifest themselves in the X-ray patterns of each sample. Figure 2(e) shows the powder XRD patterns of samples formed using a 0.3 mM HexA/methanol layer. Le Bail refinement of the patterns of HA_2PbI_4 samples we form by creating a 0.3 mM solution of hexyl amine (HexA) in methanol indicates these materials stabilize in the $P2_1/c$ monoclinic phase shown in Figure 1(b) with no evidence of any other crystalline phase, as shown in Figure S1. Calculation of the XRD pattern expected from this structure using VESTA[29] allows us to tentatively assign the planes of the material giving rise to the different peaks in the pattern we measure, which we indicate in Figure 2(e).

When we mix powders of samples formed with 0.3 and 1.5 mM HexA/methanol layers, we find the same general XRD pattern we observe in the case of the 0.3 mM sample on its own, but with different peak intensities, as seen in panel (f) of Figure 2. This similarity indicates we also form the $P2_1/c$ monoclinic phase of HA_2PbI_4 when adding 1 mL of HexA to the methanol layer. However, we believe each powdered sample possesses different amounts of preferentially oriented micro-
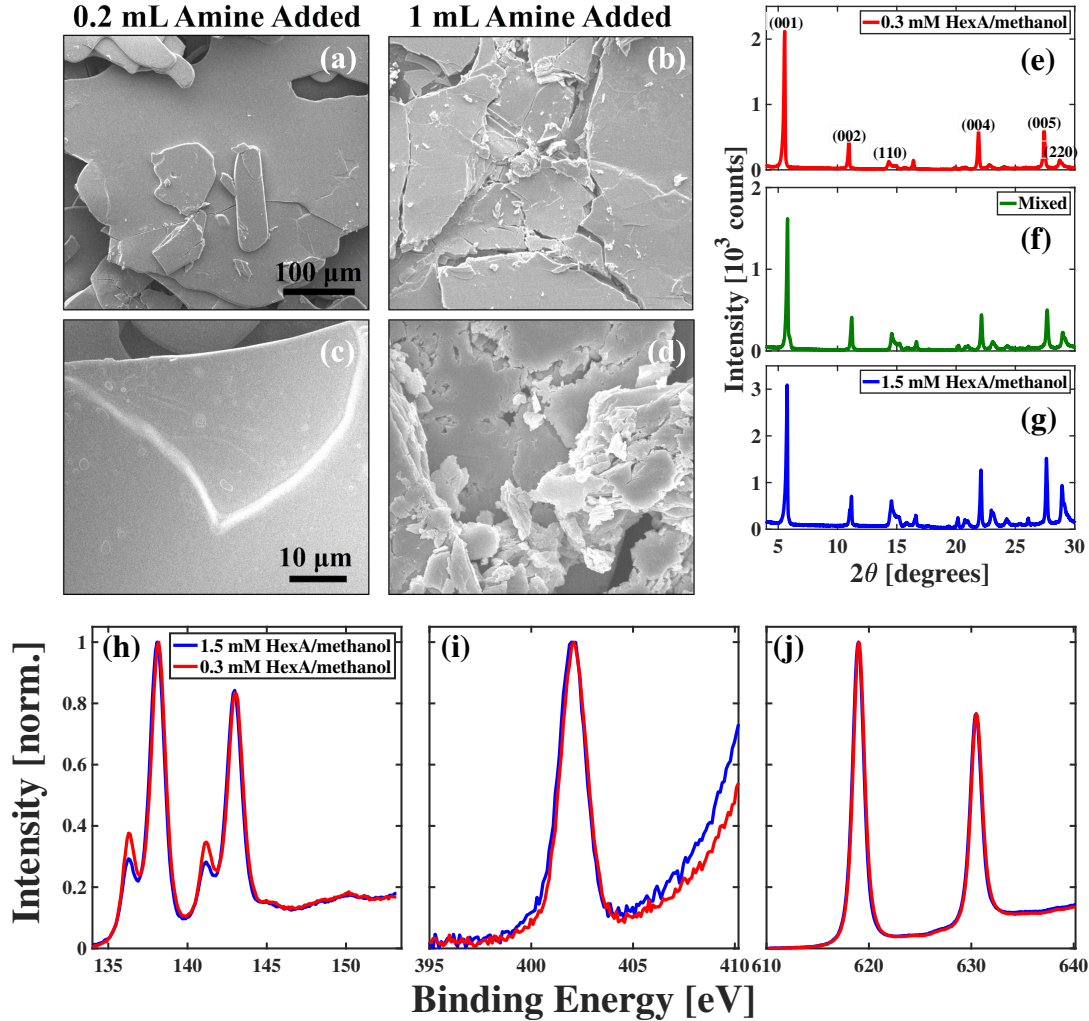
Figure 2: (a,b) SEM images of a hexyl ammonium lead iodide (HA_2PbI_4) sample formed from a 0.3 mM hexyl amine (HexA)/methanol organic solution layer at different resolutions indicating smooth edges and platy morphology of this SAQW. Scales are indicated by bars at bottom right. (b,d) SEM images of HA_2PbI_4 sample formed from a 1.5 mM HexA/methanol organic solution layer indicating rough edges and more granular morphology for the same length scales as panels (a) and (b). (e,f,g) Powder XRD patterns of HA_2PbI_4 samples formed using a 0.3 mM HexA/methanol organic layer only (e), a mixture of samples formed using the 0.3 mM and 1.5 mM HexA/methanol layers (f), and a HA_2PbI_4 sample formed from 1.5 mM HexA/methanol layer sample alone (g), indicating both samples share the same crystallographic structure. (h,i,j) Comparison between photoemission lines of Pb 4f (h), N 1s (i), and I 3d (j) of HA_2PbI_4 samples formed from 0.3 mM HexA/methanol organic layers (red) to the same lines of HA_2PbI_4 samples formed from 1.5 mM HexA/methanol organic layers (blue).

crystallites. When we inspect the patterns in panels (e) and (g) of Figure 2 we find the intensities of the higher order reflections from the (001) plane reduce significantly relative to peaks associated with reflections from other planes. In particular, we find the intensities of peaks corresponding to reflections from the (110) and (220) planes relative to those of (002) and (005), respectively, increase when one compares the patterns in panels (e) and (g) of Figure 2. Furthermore, Figure S2 shows the XRD pattern of the neat 1.5 mM sample at larger 2θ values better match those predicted for the $P2_1/c$ monoclinic phase of HA_2PbI_4 at values of 2θ between 10° and 30°. However, the relatively larger peak intensities we find for fundamental and higher order reflections from the (001) plane in the case of samples formed from the 0.3 mM HexA/methanol layers suggest the crystallites made from our powdering process remain preferentially oriented along their respective *ab* crystallographic planes. The difference in our inability to orient micro-crystallites in our sample using the same powdering technique indicates the initial morphologies of each respective sample differ in ways consistent with our findings in the SEM images. Most importantly, the preferred orientations of the micro-crystallites consistent with our XRD results suggest the samples formed using 0.3 mM HexA/methanol layers start off possessing a more platy morphology that limits our ability to powder these samples and produce more randomly oriented micro-crystallites like those we form after powdering samples made from 1.5 mM organic precursor solutions.

In contrast to the differences in the bulk morphological properties of each respective HA_2PbI_4 sample found from our SEM and XRD measurements, panels (h), (i), and (j) of Figure 2 show the local chemical bonding of the constituent atoms does not change in a significant way as we vary the chemical conditions of material formation. To establish trends between the chemical conditions of sample formation and these bonding properties we fit regions of the X-ray photoelectron spectra (XPS) characteristic of the Pb, N, and I atomic constituents of materials formed with both 0.3 mM and 1.5 mM HexA/methanol layers to model functions, as shown in Figure S3. In particular, we find XPS peaks at 138.1 eV and 143.1 eV due to $4f_{7/2}$ and $4f_{5/2}$ levels of Pb, respectively, for both samples. The splitting of these peaks indicates we observe a spin-orbit (SO) coupling of 5 eV, which is similar to 4.85 eV reported previously for octahedral coordination of the Pb site by

halogen anions in the perovskite structure.[30,31] Moreover, we find the SO splitting does not depend on the sample preparation. The other two less intense peaks observed at 141.2 eV and 136.4 eV in the XPS of Figure 2(h) stem from Pb^0 oxidation state[32,33] and indicate sample damage induced by the flux of X-rays used in the experiment. This damage occurs randomly and does not indicate systematic changes to chemical bonding of each respective material as a function of differences in precursor solutions.

In addition to using Pb photoemission features to assess the characteristics of hybrid perovskite samples, the position of the N 1s line helps confirm the formation of hybrid perovskite SAQWs.[31] As shown in Figure 2(i), we find this peak centered at 402.0 eV in our samples, which is consistent with this peak's position at 401.7 eV and 402.1 eV reported earlier in hybrid SAQW samples spaced by phenylethyl ammonium (PEA)[31] and glycine cations,[34] respectively. Close inspection of Figure 2(i) shows the N 1s peak positions do not change by amending the amount of HexA we add to our precursor solutions. Furthermore, we find no difference in the positions of photoemission peaks corresponding to the I 3d lines in our XPS studies. As shown in Figure 2(j), samples formed from 0.3 mM and 1.5 mM HexA/methanol organic layers both possess 3d peaks at 619 eV and 630.5 eV and indicate the SO coupling of 11.5 eV does not depend on the chemical conditions of HA_2PbI_4 formation. This value of the I 3d SO coupling agrees with earlier studies on hybrid perovskites.[30,35] These comparisons suggest the local chemical bonding of the bulk regions of each respective material do not change as a function of the amount of hexyl amine we use in our synthetic approach.

We further employed XPS to probe the band structures of our chemically controlled hybrid SAQW samples. The results of these measurements are shown in Figure S4. From the analysis of these spectra we obtain a valence band maximum (VBM) of 1.38 eV in both HA_2PbI_4 samples that agrees with VBM energies reported for similar 2D hybrid lead halide perovskites.[34] In addition, this VBM value in these SAQWs differs from that observed in PbI_2 powder (1.18 eV), which we discuss in the SI and show in Figure S5. The similarity between the VBM values for each material indicates the amounts of HexA we add to our precursor solutions does not affect the density of

valence band edge states in the 'bulk-like' regions of our materials. Furthermore, unlike the study of Zhu and co-workers,[8] we do not find evidence of trap states above the valence band in the observed photoemission spectra.

To gain insights into the physical origin of the broadband PL emitted by HA_2PbI_4 formed from large concentrations of amines in precursor solutions, we undertook temperature dependent light emission measurements on both types of samples. Panels (a) and (b) of Figure 3 show the results from these measurements. Inspection of the panel (a) of Figure 3 shows the intensity of the broadband emission increases by nearly 3 orders of magnitude as we cool samples formed from the 1.5 mM HexA/methanol solution to 78 K, which conforms with similar measurements we made on defective samples formed through alternative synthetic methods.[17,18] In contrast, we only observe the appearance of a weak, yet distinct broadband light emission feature when we cool a HA_2PbI_4 sample formed from the 0.3 mM HexA/methanol solution to 123 K. Additionally, we find the intensity of this feature only increases by a factor of 2 as we cool the sample to 78 K. Despite the qualitative differences in the temperature-dependent intensity of the subgap PL spectra in panels (a) and (b) of Figure 3, the fact that we observe some subgap light emission from both samples indicates the broadband PL competes with relaxation processes activated by thermal energy, as shown by Figure 3(c). Other authors have shown features similar to the subgap PL we report in this study increase significantly with decreasing temperature due to reductions in the probability of crossing over energy barriers between electronic or excitonic states.[13,21] The reduced probability of crossing these barriers subsequently lowers the participation of both competitive radiative and non-radiative relaxation channels to the photophysics of the hybrid SAQW and drives increased PL intensity.

In addition to PL measurements we undertook at different sample temperatures, we measured the broadband PL peak at several different incident laser powers while we maintained the sample temperature at 78 K. We then fit those power-dependent PL spectra to a Gaussian model of the contributing peaks and integrated the subsequent model functions over the photon wavelengths we detected experimentally. Comparisons between the measured and fitted spectra can be found in
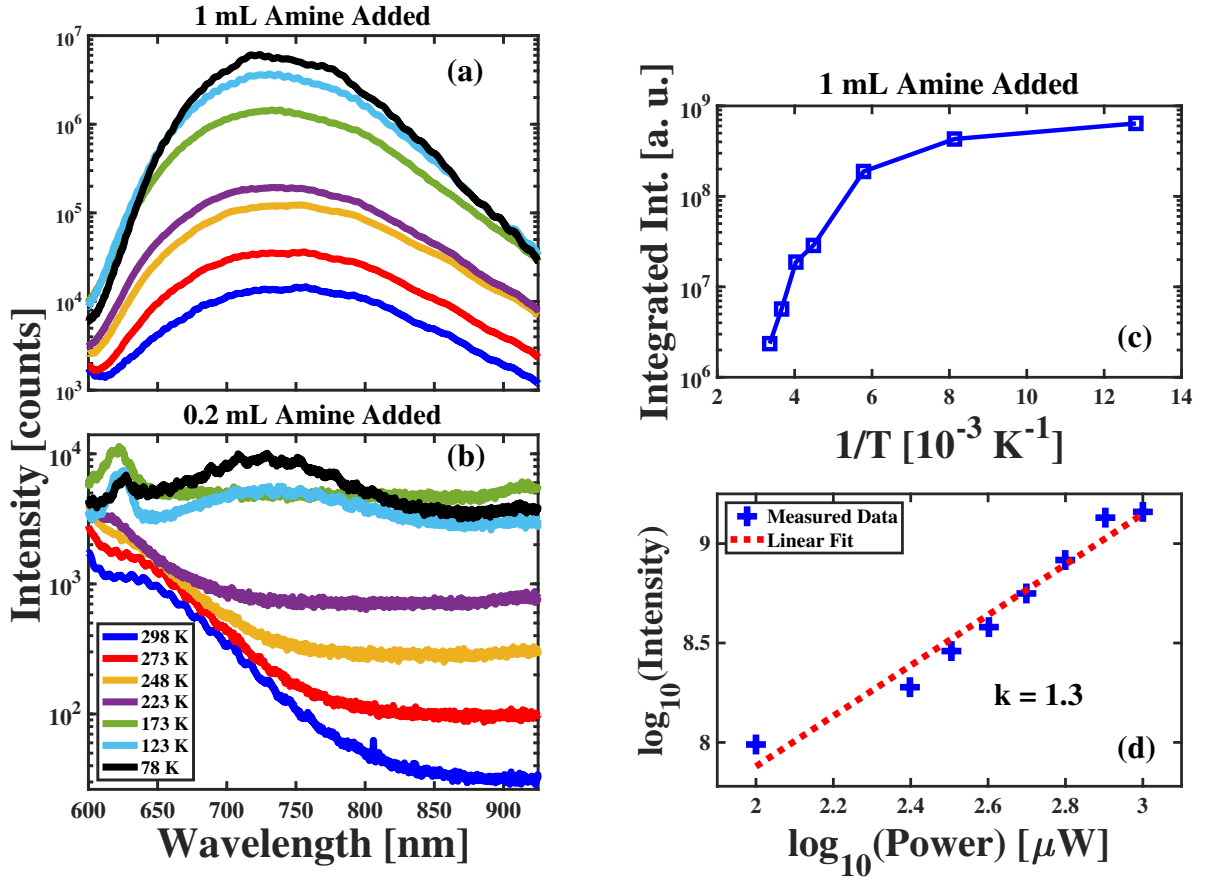
Figure 3: (a,b) Temperature dependent photoluminescence spectra of a hexyl ammonium lead iodide (HA$_2$PbI$_4$) samples formed from 1.5 mM (a) and 0.3 mM (b) hexyl amine (HexA)/methanol organic layers. (c) Temperature dependent integrated intensity of the broadband light spectrum emitted by a HA$_2$PbI$_4$ sample formed from a 1.5 mM HexA/methanol organic layer showing plateau-like behavior at low temperatures. (d) Power dependence of the broadband subgap photoluminescence emitted by a HA$_2$PbI$_4$ sample formed from a 1.5 mM HexA/methanol organic layer showing a slope value greater than 1 indicating the concentration of donor/acceptor sites participate in the light emission mechanism.

Figure S6. As established through the kinetic modeling of the light emission process by Schmidt et al, we can tentatively assign the type of electronic state driving our observation of broadband subgap PL from HA_2PbI_4 samples by plotting the integrated PL intensity as a function of the incident laser power on base-10 logarithmic scales.[36] In particular, Schmidt et al. showed that by driving the exciton transition resonantly one expects the log-log plot of PL signals caused by both free and bound excitons against laser power will be lines with unity slopes when light absorption does not change the number of electron donor or acceptor sites in the material. However, if the number of acceptor or donor sites does change as a function of the incident laser power, then one can observe log-log power-PL plots corresponding to bound excitons whose slopes exceed 1 even under resonant photoexcitation of the free exciton state. Specifically, we should find a slope of 1+k where k is the exponential value of the power dependence of donor/acceptor site number in the sample. Using these physical insights into the power-dependent trend of the integrated PL intensity, we can fit our results to a line and not only assess what kind of electronic excitation drives our observations, but also investigate other dynamical processes consistent with our experimental results. In particular, if the slope of the log-log plot exceeds 1, then one can conclude tentatively the PL feature in the analyzed spectrum stems from an exciton bound to a donor or acceptor site whose concentration must change as the density of free excitons increases.

Panel (d) of Figure 3 shows we find a line possessing a slope of 1.3 fits our experimental log-log power-PL plot. Given its value is larger than 1, the slope of the power-dependent PL spectra indicates two physical processes participate in the light emission process. First, since we excite the sample on resonance with the exciton absorption peak, the slope value suggests the number of electron donor and/or acceptor sites in our samples changes as we increase the power of the incident laser source. Specifically, given the relation we detailed above, we expect the number of donor/acceptor sites possess a sublinear power dependence with an exponential value near 0.3. Second, the larger than unity slope of the power dependence in Figure 3(d) indicates the subgap PL emitted by HA_2PbI_4 formed using the 1.5 mM HexA/methanol layers results from an exciton bound to a defect site that acts as an electron donor or acceptor.
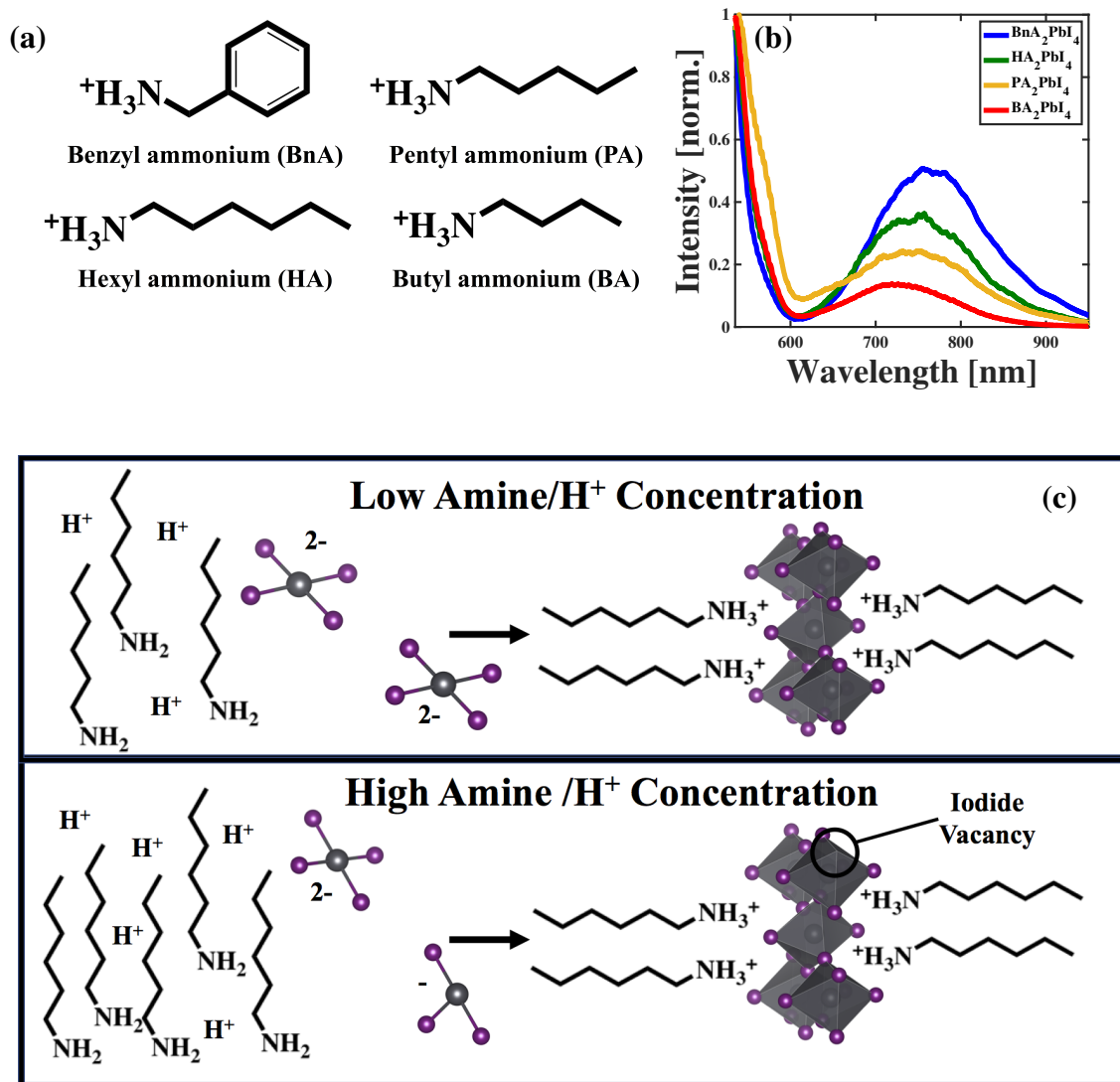
Figure 4: (a) Structures and names of cations we used to make defective SAQWs capable of emitting broadband light spectra at room temperature. (b) Comparison between the room temperature subgap photoluminescence (PL) emitted from BnA_2PbI_4 (blue), HA_2PbI_4 (green), PA_2PbI_4 (yellow) and BA_2PbI_4 (red) showing similar widths and positions between the different peaks. (c). Top panel: the chemical mechanism we propose occurs under low amine/H^+ concentrations to form a high density of pristine SAQW primitive cells incapable of emitting broadband PL at room temperature. Bottom panel: the chemical mechanism we propose occurs under high amine/H^+ concentrations to form a sufficient density of I^- vacancies that we observe broadband PL emission at room temperature

We extended our synthetic method to chemically control the subgap light emission of hybrid SAQW samples spaced by three additional molecular cations whose structures are shown in Figure 4(a). This extension allows us to assess the generalizability of our approach and helps us assign what defects give rise to the broadband subgap PL spectra. Specifically, we formed butyl ammonium lead iodide (BA_2PbI_4), pentyl ammonium lead iodide (PA_2PbI_4), and benzyl ammonium lead iodide (BnA_2PbI_4) under similar conditions to those we described above for the case of HA_2PbI_4. We detail the structures of these materials in the SI. As seen in Figure 4(b), we can successfully form materials whose subgap PL spectra resemble that of HA_2PbI_4 formed under high amine concentrations. In particular, we find all four of the materials shown in Figure 4(b) emit subgap PL spectra containing broad features whose peaks can be found near 750 nm. Table 1 reports the peak wavelength, λ_{max}, and width, $\Delta\lambda$, in units of nm for each of the broad features in Figure 4(b), which we extract using an asymmetric model of the peak shape indicative of non-negligible surface roughness in our samples.[18] The similar values for the peak wavelengths of the broadband PL we report in Table 1 indicate increasing the concentration of amine in the organic solution of our layered synthetic approach acts a general chemical lever one can use to control the light emission spectra of hybrid SAQW materials. Furthermore, the relatively small effect different cations make on both the peak positions and broad width of the spectra in Figure 4(b) suggests defects form in the inorganic layers and dominate exciton trapping. However, the spectra in Figures 1 and 3 do not clarify the chemical mechanism through which defects form in these inorganic layers using our synthetic approach.

Table 1: Comparison between the values of the peak maximum, λ_{max}, and width, $\Delta\lambda$, of subgap photoluminescence emitted at 298 K by hybrid SAQW samples spaced by different molecular cations.

molecular cation	λ_{max} (nm)	$\Delta\lambda$ (nm)
butyl ammonium	729.1$\pm$1.0	95.6$\pm$1.0
pentyl ammonium	738.0 $\pm$0.6	108.1$\pm$0.8
hexyl ammonium	744.9$\pm$0.5	95.2$\pm$0.4
benzyl ammonium	760.2$\pm$0.4	95.2$\pm$0.6

To understand the mechanism of light emissive defect chemistry we assess the fundamental

chemical processes controlling material formation. Under optimal conditions we propose the formation of our hybrid SAQW samples results from controlling the following chemical equilibrium,

$$2\,\text{HexA} + 2\,\text{H}^+ + \text{PbI}_4^{2-} \rightleftharpoons \text{HA}_2\text{PbI}_4,$$

where the PbI_4^{2-} polyiodide species corresponds to the fully coordinated polyhedron necessary to form a pristine primitive cell of HA_2PbI_4. As we push the above equilibrium towards its product side the fully coordinated PbI_4^{2-} will be consumed and need to be replenished by coordinating an additional iodide to the PbI_3^- species. From this perspective one must balance the equilibrium constants for the ammonium protonation and iodide coordination processes carefully to properly maintain the necessary concentration of PbI_4^{2-} to continue forming the pristine primitive cell. Initial experiments by Mitzi showed maintaining a stoichiometric balance between the reactants results in extremely slow material formation over the course of many months in the case of PEA lead chloride.[37] However, if one adds too much of the amine and proton to their respective solution layers, then one can tip the equilibrium too strongly in favor of the products so that it becomes,

$$4\,\text{HexA} + 4\,\text{H}^+ + \text{PbI}_4^{2-} + \text{PbI}_3^- \rightleftharpoons \text{HA}_2\text{PbI}_4 + \text{HA}_2\text{PbI}_3^+,$$
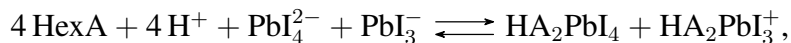
where we consider formation of a defective SAQW sample $\text{HA}_2\text{PbI}_3^+$ from the incompletely coordinated PbI_3^- polyiodide species. We propose our chemical method of adding excess amine to the organic solution layer drives formation of too much molecular cation to balance the complex equilibria of SAQW self-assembly and causes defective regions to form in our samples.

To test this hypothesis, we synthesized HA_2PbI_4 samples by replacing 1/3 of the HI content in the aqueous layer with the stoichiometrically appropriate amount of sodium iodide (NaI). The NaI dissolves completely in the aqueous layer and allows us to maintain the same concentration of I^- in the inorganic solution while decreasing $[\text{H}^+]$. Since we maintain the same concentration of I^- in the aqueous layer, we predict the relative amounts of PbI_3^- and PbI_4^{2-} polyiodide species in the inorganic solution will remain unchanged when compared to the case when we use only HI in this layer.[38] The identical UV-vis absorption spectra of our different precursor solutions shown in Figure S7 in the region where we expect characteristic polyiodide transitions shows the NaI/HI

solution drives formation of the same concentration of the polyiodide species we find in fully HI solutions.

Despite the formation of the same concentrations of the polyiodide species necessary to drive the equilibria above towards product formation, we find the subgap PL spectra differ substantially when comparing materials formed from aqueous solutions containing different H^+ concentrations. Figure S8 shows the representative temperature dependent subgap PL spectra we find emitted by HA_2PbI_4 samples formed from these NaI/HI/PbI$_2$ aqueous solutions in the presence of a 1.5 mM HexA/methanol layer. These spectra show that in spite of the fact we have loaded the organic solution with a large amount of the amine, we find minimal broadband, subgap PL similar to the spectra we measure under low amine concentrations, as shown in Figure 3(b). This comparison suggests that reducing the H^+ concentration in the inorganic solution layer reduces the chemical forces toward product formation in the equilibria described above and slows down the crystallization process enough that we do not form a sufficient number of defective sites to cause significant broadband subgap PL, especially at room temperature.

Based on the variation of the subgap PL as we change both the amine and H^+ concentrations, we propose we can control the formation of defective primitive cells by controlling the kinetics of the chemical equilibria described above. We highlight our proposed mechanism of defect formation under different cation conditions schematically in Figure 4(c). Under lower amine or H^+ concentrations, the available amine gets protonated more slowly and forms crystallites with more of the fully coordinated PbI_4^{2-} polyiodide species, as shown in the top panel of Figure 4(c). In contrast, the bottom panel of Figure 4(c) shows when we increase the concentration of amine in the organic layer and H^+ concentration in the aqueous solution layer, significantly more of the amine molecules near the liquid-liquid interface become protonated. The higher relative concentration of ammonium cations at the liquid-liquid interface drives the self-assembly processes more strongly toward the products. This driving force then increases the probability of forming SAQW crystals with the incompletely coordinated polyiodide species PbI_3^-, which produces I^- vacancies. This picture of the mechanism of defect formation in our samples helps explain the differences between

the morphological properties of samples formed under different cation concentrations.

Our morphology studies using SEM and XRD described above suggest that high amine/H$^+$ concentrations prevent achieving long-range order within the ab-plane of HA$_2$PbI$_4$. This inability to form ordered structures indicates the ammonium cations coordinate Pb-bound iodides of the PbI$_3^-$ species such that large densities of I$^-$ vacancies form in the equatorial plane of the octahedral sheet, as shown in the bottom panel of Figure 4(c). When enough of these vacancies form together they organize into edge states in the ab-plane and terminate crystal growth. This growth termination leads to the formation of smaller, more granular SAQW crystallites relative to the large plates formed under low amine/H$^+$ concentrations and allows us to make powders possessing fewer preferentially oriented plates.

The appearance of single or collective I$^-$ equatorial vacancies also helps us explain specific dynamical processes imparted on our power-dependent PL measurements. As we detailed above, the slope of the line we find by analyzing the log-log plot of the power-dependent subgap PL emitted from HA$_2$PbI$_4$ formed under high cation concentrations suggests this broadband spectral feature corresponds to an exciton bound at a defect capable of acting like an electron donor or acceptor site. The I$^-$ vacancies we propose form from accelerating the self-assembly should act as effective electron donating sites due to the incomplete coordination of the Pb cation of the PbI$_3^-$ polyiodide species. If this donating site traps the hole contribution to the free exciton, then the increased formation of photoexcited excitons as we increase our incident laser power should cause a decrease in available donor sites in the sample per absorbed photon relative to the case of lower incident laser powers. This situation should produce a sublinear power dependence on the number of electron donating sites, like the one we find consistent with our experimental power-dependent PL results described above. This consistency between the expected physical mechanism driving exciton trapping in the presence of excess electron donating sites in the form of I$^-$ vacancies and the findings from our power-dependent PL measurements further validates our proposed chemical mechanism of defect formation.

Furthermore, the broad bandwidth of the subgap PL also implicates collective I$^-$ vacancies,

which likely form into edge states. Previous computational studies show the appearance of broadband features in the PL spectra of hybrid and fully organic lead halide perovskites stems from the formation of low dimensional structures whose stability cannot be maintained in the presence of an exciton.[39] Given this and similar results in materials classes such as psuedo-1D halide-bridge mixed-valence transition complexes,[40–44] we propose one observes broadband subgap PL from our hybrid SAQW samples when a sufficiently high density of I$^-$ vacancies form and produce collective states whose structures are unstable to the presence of the free exciton. To test this hypothesis we compared the subgap PL of HA$_2$PbI$_4$ samples formed with 1.5 mM HexA/methanol organic and fully concentrated HI aqueous solutions, respectively, before and after powdering the sample using the same methods employed for our XRD measurements, as seen in Figure S11. This comparison shows the powdering process quenches the broadband subgap PL intensity we measure at room temperature and causes a blueshift of the broad spectrum at low temperature. These changes in the characteristics of the light emission spectra of our defective HA$_2$PbI$_4$ samples as a function of processing them into smaller crystallites further confirm our proposal that collective defective regions of our samples, such as edge states, cause exciton trapping and drive our observation of broadband PL at room temperature.

While several studies examine the electronic structure of defective hybrid SAQWs using density functional theory (DFT) methods,[13,15,19–21,39,45] our experimental results indicate similar calculations would not yield results physically meaningful to determine what electronic states participate in fundamental mechanisms of subgap PL in our samples. Specifically, DFT methods cannot account for excitonic excitations in the band structure predicted for specific materials. Since variation in the PL spectra as a function of incident laser power and molecular cation indicate broadband light emission stems from excitons bound to I$^-$ vacancies, we do not expect DFT calculations to accurately predict the energy of the state from which light emission occurs in our samples. One would need to undertake GW calculation in combination with techniques such as the Bethe-Salpeter equation. However, due to the complexity of the unit cells corresponding to materials we have synthesized and large supercells necessary to accurately model the density of collective

defects in our samples, these state-of-the-art calculations are beyond our capabilities currently.

In conclusion, we have used control over molecular cation concentrations at the liquid-liquid interface of a layered solution synthetic approach to modulate the subgap photoluminescence spectra of several hybrid organic lead iodide self-assembled quantum well samples. We found that forming materials with precursor solutions containing different concentrations of molecular cations drives differences in both the presence of substantial room temperature broadband light emission and the morphological features of these samples. Photoluminescence spectroscopic studies undertaken as a function of sample temperature and incident laser power suggest broad features in the subgap PL spectra result from exciton self-trapping at defect sites. We use simple analysis of the chemical equilibria we propose controls materials formation to argue high cation concentrations drive the formation of SAQW samples from incompletely coordinated Pb polyiodide species that preferentially coordinate electron donating I^- vacancies into the equatorial plane of defective materials. Based on previous computational studies of self-trapped excitons in similar hybrid SAQW samples, we propose these vacancies form collective edge states at sufficiently high cation concentrations whose structure becomes unstable to the presence of the free exciton, causes exciton trapping, and drives broadband light emission. These results highlight the important role molecular cations can play in the formation of hybrid SAQW materials with controlled optoelectronic properties for applications like solution-processed near-infrared surveillance technologies.

Acknowledgement

Supporting Information Available

Supplemental Information including experimental methods, results from the Le Bail refinement of powder X-ray diffraction pattern, fits to the XPS data, band structures of our SAQWs, fits to power-dependent PL, structural and optical measurements on analogue SAQWs can be found online at:

References

(1) Mao, L.; Wu, Y.; Stoumpos, C. C.; Wasielewski, M. R.; Kanatzidis, M. G. White-Light Emission and Structural Distortion in New Corrugated Two-Dimensional Lead Bromide Perovskites. *J. Am. Chem. Soc.* **2017**, *139*, 5210–5215.

(2) Smith, M. D.; Karunadasa, H. I. White-Light Emission from Layered Halide Perovskites. *Acc. Chem. Res.* **2018**, *51*, 619–627.

(3) Hu, T.; Smith, M. D.; Dohner, E. R.; Sher, M.-J.; Wu, X.; Trinh, M. T.; Fisher, A.; Corbett, J.; Zhu, X.-Y.; Karunadasa, H. I.; Lindenberg, A. M. Mechanism for Broadband White-Light Emission from Two-Dimensional (110) Hybrid Perovskites. *J. Phys. Chem. Lett.* **2016**, *7*, 2258–2263.

(4) Wang, N. et al. Perovskite Light-Emitting Diodes Based on Solution-Processed Self-Organized Multiple Quantum Wells. *Nat. Photon.* **2016**, *10*, 699.

(5) Veldhuis, S. A.; Boix, P. P.; Yantara, N.; Li, M.; Tze, C. S.; Mathews, N.; Mhaisalkar, S. G. Perovskite Materials for Light-Emitting Diodes and Lasers. *Adv. Mater.* **2016**, *28*, 6804–6834.

(6) Chang, J.; Zhang, S.; Wang, N.; Sun, Y.; Wei, Y.; Li, R.; Yi, C.; Wang, J.; Huang, W. Enhanced Performance of Red Perovskite Light-Emitting Diodes through the Dimensional Tailoring of Perovskite Multiple Quantum Wells. *J. Phys. Chem. Lett.* **2018**, *9*, 881–886.

(7) Liu, X.-K.; Gao, F. Organic-Inorganic Hybrid Ruddlesden-Popper Perovskites: An Emerging Paradigm for High-Performance Light-Emitting Diodes. *J. Phys. Chem. Lett.* **2018**, *9*, 2251–2258.

(8) Wu, X.; Trinh, M. T.; Niesner, D.; Zhu, H.; Norman, Z.; Owen, J. S.; Yaffe, O.; Kudisch, B. J.; Zhu, X. Y. Trap States in Lead Iodide Perovskites. *J. Am. Chem. Soc.* **2015**, *137*, 2089–2096.

(9) Milot, R. L.; Sutton, R. J.; Eperon, G. E.; Haghighirad, A. A.; Hardigree, J. M.; Miranda, L.; Snaith, H. J.; Johnston, M. B.; Herz, L. M. Charge-Carrier Dynamics in 2D Hybrid Metal - Halide Perovskites. *Nano Lett.* **2016**, *16*, 7001–7007.

(10) Stoumpos, C. C.; Cao, D. H.; Clark, D. J.; Young, J.; Rondinelli, J. M.; Jang, J. I.; Hupp, J. T.; Kanatzidis, M. G. Ruddlesden-Popper Hybrid Lead Iodide Perovskite 2D Homologous Semiconductors. *Chem. Mat.* **2016**, *28*, 2852–2867.

(11) Straus, D. B.; Kagan, C. R. Electrons, Excitons, and Phonons in Two-Dimensional Hybrid Perovskites: Connecting Structural, Optical, and Electronic Properties. *J. Phys. Chem. Lett.* **2018**, *9*, 1434–1447.

(12) Yaffe, O.; Chernikov, A.; Norman, Z. M.; Zhong, Y.; Velauthapillai, A.; Van Der Zande, A.; Owen, J. S.; Heinz, T. F. Excitons in Ultrathin Organic-Inorganic Perovskite Crystals. *Phys. Rev. B - Cond. Matt. Mat. Phys.* **2015**, *92*, 045414.

(13) Kahmann, S.; Tekelenburg, E. K.; Duim, H.; Kamminga, M. E.; Loi, M. A. Extrinsic nature of the broad photoluminescence in lead iodide-based Ruddlesden-Popper perovskites. *Nat. Comm.* **2020**, *11*, 2344.

(14) Dohner, E. R.; Jaffe, A.; Bradshaw, L. R.; Karunadasa, H. I. Intrinsic White-Light Emission from Layered Hybrid Perovskites. *J. Am. Chem. Soc.* **2014**, *136*, 13154–13157.

(15) Cortecchia, D.; Neutzner, S.; Ram, A.; Kandada, S.; Mosconi, E.; Meggiolaro, D.; Angelis, F. D.; Soci, C.; Petrozza, A. Broadband Emission in Two-Dimensional Hybrid Perovskites: The Role of Structural Deformation. *J. Am. Chem. Soc.* **2017**, *139*, 39–42.

(16) Zhang, Q.; Ji, Y.; Chen, Z.; Vella, D.; Wang, X.; Xu, Q.-H.; Li, Y.; Eda, G. Controlled Aqueous Synthesis of 2D Hybrid Perovskites with Bright Room-Temperature Long-Lived Luminescence. *J. Phys. Chem. Lett.* **2019**, *10*, 2869–2873.

(17) Sanni, A. M.; Lavan, S. N.; Avramenko, A.; Rabuffetti, F. A.; Suescun, L.; Rury, A. S. Room-Temperature Broadband Light Emission from Hybrid Lead Iodide Perovskite-Like Quantum Wells: Terahertz Spectroscopic Investigation of Metastable Defects. *J. Phys. Chem. Lett.* **2019**, *10*, 1653–1662.

(18) Sanni, A. M.; Shuhag, S.; Rury, A. S. Probing Fabry–Perot Interference in Self-Assembled Excitonic Microcrystals with Subgap Light Emission. *J. Phys. Chem. C* **2019**, *123*, 23103–23112.

(19) Yin, J.; Naphade, R.; Gutiérrez Arzaluz, L.; Brédas, J.-L.; Bakr, O. M.; Mohammed, O. F. Modulation of Broadband Emissions in Two-Dimensional $< 100 >$-Oriented Ruddlesden-Popper Hybrid Perovskites. *ACS Energy Lett.* **2020**, *0*, 2149–2155.

(20) Booker, E. P.; Thomas, T. H.; Quarti, C.; Stanton, M. R.; Dashwood, C. D.; Gillett, A. J.; Richter, J. M.; Pearson, A. J.; Davis, N. J. L. K.; Sirringhaus, H.; Price, M. B.; Greenham, N. C.; Beljonne, D. Formation of Long-Lived Color Centers for Broadband Visible Light Emission in Low-Dimensional Layered Perovskites. *J. Am. Chem. Soc.* **2017**, *139*, 18632–18639.

(21) Li, T.; Chen, X.; Wang, X.; Lu, H.; Yan, Y.; Beard, M. C.; Mitzi, D. B. Origin of Broad-

Band Emission and Impact of Structural Dimensionality in Tin-Alloyed Ruddlesden–Popper Hybrid Lead Iodide Perovskites. *ACS Energy Lett.* **2020**, *5*, 347–352.

(22) Park, D. Y.; An, S.-J.; Lee, C.; Nguyen, D. A.; Lee, K.-N.; Jeong, M. S. Investigation of Chemical Origin of White-Light Emission in Two-Dimensional $(C_4H_9NH_3)_2PbBr_4$ via Infrared Nanoscopy. *J. Phys. Chem. Lett.* **2019**, *10*, 7942–7948.

(23) Yangui, A.; Garrot, D.; Lauret, J. S.; Lusson, A.; Bouchez, G.; Deleporte, E.; Pillet, S.; Bendeif, E. E.; Castro, M.; Triki, S.; Abid, Y.; Boukheddaden, K. Optical Investigation of Broadband White-Light Emission in Self-Assembled Organic–Inorganic Perovskite $(C_6H_{11}NH_3)_2PbBr_4$. *J. Phys. Chem. C* **2015**, *119*, 23638–23647.

(24) Kang, J.; Wang, L.-W. Dynamic Disorder and Potential Fluctuation in Two-Dimensional Perovskite. *J. Phys. Chem. Lett.* **2017**, *8*, 3875–3880.

(25) Yangui, A.; Roccanova, R.; McWhorter, T. M.; Wu, Y.; Du, M.-H.; Saparov, B. Hybrid Organic–Inorganic Halides $(C_5H_7N_2)_2MBr_4$ (M = Hg, Zn) with High Color Rendering Index and High-Efficiency White-Light Emission. *Chem. Mat.* **2019**, *31*, 2983–2991.

(26) Shi, E.; Deng, S.; Yuan, B.; Gao, Y.; Akriti,; Yuan, L.; Davis, C. S.; Zemlyanov, D.; Yu, Y.; Huang, L.; Dou, L. Extrinsic and Dynamic Edge States of Two-Dimensional Lead Halide Perovskites. *ACS Nano* **2019**, *13*, 1635–1644.

(27) Qin, Z. et al. Spontaneous Formation of 2D/3D Heterostructures on the Edges of 2D Ruddlesden–Popper Hybrid Perovskite Crystals. *Chem. Mat.* **2020**, *32*, 5009–5015.

(28) Zhao, C.; Tian, W.; Sun, Q.; Yin, Z.; Leng, J.; Wang, S.; Liu, J.; Wu, K.; Jin, S. Trap-Enabled Long-Distance Carrier Transport in Perovskite Quantum Wells. *J. Am. Chem. Soc.* **2020**, *142*, 15091–15097.

(29) Momma, K.; Izumi, F. *VESTA3* for Three-Dimensional Visualization of Crystal, Volumetric and Morphology Data. *J. Appl. Crystallogr* **2011**, *44*, 1272–1276.

(30) Philippe, B.; Park, B.-W.; Lindblad, R.; Oscarsson, J.; Ahmadi, S.; Johansson, E. M. J.; Rensmo, H. Chemical and Electronic Structure Characterization of Lead Halide Perovskites and Stability Behavior under Different Exposures—A Photoelectron Spectroscopy Investigation. *Chem. Mat.* **2015**, *27*, 1720–1731.

(31) Gan, L.; He, H.; Li, S.; Li, J.; Ye, Z. Distinctive excitonic recombination in solution-processed layered organic–inorganic hybrid two-dimensional perovskites. *J. Mater. Chem. C* **2016**, *4*, 10198–10204.

(32) McGettrick, J. D.; Hooper, K.; Pockett, A.; Baker, J.; Troughton, J.; Carnie, M.; Watson, T. Sources of Pb(0) artefacts during XPS analysis of lead halide perovskites. *Mater. Lett.* **2019**, *251*, 98 – 101.

(33) Béchu, S.; Ralaiarisoa, M.; Etcheberry, A.; Schulz, P. Photoemission Spectroscopy Characterization of Halide Perovskites. *Adv. Energy Mater* **2020**, *10*, 1904007.

(34) Zhang, Q.; Zhao, J.; Xiao, Z.; Zhou, J.; Hong, B.; Luo, Z.; Bao, J.; Gao, C. Improved Moisture Stability of 2D Hybrid Perovskite (HOOC–CH$_2$–NH$_3$)$_2$PbI$_4$ by Dehydration Condensation between Organic Components. *ACS Appl. Energy Mater.* **2018**, *1*, 2502–2511.

(35) Lindblad, R.; Bi, D.; Park, B.-w.; Oscarsson, J.; Gorgoi, M.; Siegbahn, H.; Odelius, M.; Johansson, E. M. J.; Rensmo, H. Electronic Structure of TiO2/CH$_3$NH$_3$PbI$_3$ Perovskite Solar Cell Interfaces. *J. Phys. Chem. Lett.* **2014**, *5*, 648–653.

(36) Schmidt, T.; Lischka, K.; Zulehner, W. Excitation-power Dependence of the Near-band-edge Photoluminescence of Semiconductors. *Phys. Rev. B - Cond. Matt. Mat. Phys.* **1992**, *45*, 8989–8994.

(37) Mitzi, D. A Layered Solution Crystal Growth Technique and the Crystal Structure of (C$_6$H$_5$C$_2$H$_4$NH$_3$)$_2$PbCl$_4$. *J Solid State Chem.* **1999**, *145*, 694 – 704.

(38) Mastria, R.; Colella, S.; Qualtieri, A.; Listorti, A.; Gigli, G.; Rizzo, A. Elucidating the effect of the lead iodide complexation degree behind the morphology and performance of perovskite solar cells. *Nanoscale* **2017**, *9*, 3889–3897.

(39) Wang, X.; Meng, W.; Liao, W.; Wang, J.; Xiong, R.-G.; Yan, Y. Atomistic Mechanism of Broadband Emission in Metal Halide Perovskites. *J. Phys. Chem. Lett.* **2019**, *10*, 501–506.

(40) Gammel, J. T.; Saxena, A.; Batistić, I.; Bishop, A. R.; Phillpot, S. R. Two-band model for halogen-bridged mixed-valence transition-metal complexes. I. Ground state and excitation spectrum. *Phys. Rev. B - Cond. Matt. Mat. Phys.* **1992**, *45*, 6408–6434.

(41) Ku, L.-C.; Trugman, S. A. Quantum dynamics of polaron formation. *Phys. Rev. B - Cond. Matt. Mat. Phys.* **2007**, *75*, 014307.

(42) Fehske, H.; Wellein, G.; Bishop, A. R. Spatiotemporal evolution of polaronic states in finite quantum systems. *Phys. Rev. B - Cond. Matt. Mat. Phys.* **2011**, *83*, 075104.

(43) Golež, D.; Bonča, J.; Vidmar, L.; Trugman, S. A. Relaxation Dynamics of the Holstein Polaron. *Phys. Rev. Lett.* **2012**, *109*, 236402.

(44) Mance, J. G.; Felver, J. J.; Dexheimer, S. L. Observation of structural relaxation during exciton self-trapping via excited-state resonant impulsive stimulated Raman spectroscopy. *J. Chem. Phys.* **2015**, *142*, 084309.

(45) Cortecchia, D.; Yin, J.; Bruno, A.; Lo, S.-Z. A.; Gurzadyan, G. G.; Mhaisalkar, S.; Brédas, J.-L.; Soci, C. Polaron Self-Localization in White-Light Emitting Hybrid Perovskites. *J. Mater. Chem. C* **2017**, *5*, 2771–2780.

Graphical TOC Entry